

https://dspace.org/

Dynamics of a susceptibleinfectedrecovered model on complex networks with interregional migration

Ruiwu Niu; Yin-Chi Chan; Eric W.M Wong; Michael Van Wyk; Simin Lui

AMER PHYSICAL SOC
https://hdl.handle.net/10539/43429
WOS

Downloaded from a DSpace repository. https://dspace.org/

Dynamics of a susceptible-infected-recovered model on complex networks with interregional migration

Ruiwu Niu
Department of Electrical Engineering, City University of Hong Kong, 83 Tat Chee Avenue, Kowloon Tong, Hong Kong

Yin-Chi Chan
Institute for Manufacturing, University of Cambridge, 17 Charles Babbage Road, Cambridge CB3 0FS, United Kingdom

Eric W. M. Wong*
Department of Electrical Engineering, City University of Hong Kong, 83 Tat Chee Avenue, Kowloon Tong, Hong Kong

Michaël Antonie van Wyk†
School of Electrical and Information Engineering, University of the Witwatersrand, Johannesburg 2000, South Africa

Simin Liu
Department of Electrical Engineering, City University of Hong Kong, 83 Tat Chee Avenue, Kowloon Tong, Hong Kong

(Received 29 September 2023; accepted 2 July 2024; published 6 August 2024)

We present a susceptible-infected-recovered model based on a dynamic flow network that describes the epidemic process on complex metapopulation networks. This model views population regions as interconnected nodes and describes the evolution of each region using a system of differential equations. The next-generation matrix method is used to derive the global basic reproduction number for three cases: a general network with homogeneous infection rates in all regions, a fully connected network, and a star network with heterogeneous infection and recovery rates. For the homogeneous case, we show that this global basic reproduction number is independent of the migration rates between regions. However, the rate of convergence of each region to an equilibrium state exhibits a much larger variance in random (Erdős-Rényi) networks compared to small-scale (Barabási-Albert) networks. For the general heterogeneous case, we report interesting results, namely that the global basic reproduction number decays exponentially with respect to the smallest nonzero Laplacian eigenvalue (algebraic connectivity). Furthermore, we demonstrate both analytically and numerically that as the network's algebraic connectivity increases, either by increasing the average node degree of each region or the global migration rate, the global basic reproduction number decreases and converges to the ratio of the average local infection rate to the average local recovery rate, meaning that the lower bound of the global basic reproduction rate does not equal the mean of local basic reproduction rates.

DOI: 10.1103/PhysRevE.110.024304

I. INTRODUCTION

Over the past several years, the world has painfully endured the COVID-19 pandemic. Although COVID-19 is no longer a public health emergency of international concern [1], vigilance is still required to defend against future pandemics [2,3]. In particular, accurate epidemiological modeling is required to predict the spread of diseases and formulate appropriate responses.

An early example of an epidemiological model is the classic susceptible-infected-recovered (SIR) compartmental model by Kermack and McKendrick [4]. Similar models include the susceptible-infected-susceptible (SIS) and susceptible-infected-recovered-susceptible (SIRS) models for the cases in which recovery from infection provides no immunity and time-limited immunity from reinfection, respectively, and the susceptible-exposed-infected-recovered (SEIR) model, where exposed individuals undergo a latent period before becoming infectious [5,6]. Note that these models are all *mean-field* models, which assume full mixing of the population. Due to their simplicity, mean-field models remain prevalent in epidemic modeling; for example, mean-field compartmental models were used in [7–9] to model the spread of COVID-19. In particular, Ref. [7] considered migration, but only between a "local" region and the "rest of the world."

A. Epidemic models on networks

The mean-field approach model cannot deal with epidemics' *microscopic-level* (agent-based) movements on

*Contact author: eeewong@cityu.edu.hk
†Also at: Department of Electrical Engineering, City University of Hong Kong, 83 Tat Chee Avenue, Kowloon Tong, Hong Kong.

 ©2024 American Physical Society

heterogeneous structures despite its simplicity and usefulness. With the rise of network science [10–12], scientists started to combine epidemic models with complex networks to study how heterogeneous connections influence the epidemic process [13]. By using percolation models and generating function methods, Newman solved a class of SIR models on a variety of networks [14]. For heterogeneous networks, such as scale-free networks, Pastor-Satorras and Vespignani found that the effective epidemic threshold is close to zero when the network size is huge [15]. In addition, considering the propagation of information during the spreading process of the disease, Granell *et al.* proposed a multilayer compartmental model and found that transparent information can restrain the spreading of the disease [16]. Subsequently, Wei *et al.* found that the interlayer links could promote the epidemic spreading on interconnected networks [17].

However, such microscopic-level models are too complicated and resource-intensive for describing *macroscopic-level* movements between regions (districts, cities, and states) [18]. As a result, coarse-grained metapopulation models were developed by considering geographically distributed populations as different nodes, and human flows as links between nodes [19–30]. Most models are based on so-called reaction-diffusion processes regarding human traffic flows among nodes as a diffusion process [20–22,25–30]. Colizza *et al.* gave out the derivation of basic reaction-diffusion equations describing the metapopulation system at the mechanistic level and the discovery of a global threshold for subpopulation invasion [22]. Reference [25] discussed the effects of diffusion rates on epidemic spreads in metapopulation networks, and it showed that diffusion could suppress epidemics by increasing the epidemic threshold. Reference [31] proposed a theoretical framework for studying spreading processes in structured metapopulations with heterogeneous agents subjected to different recurrent mobility patterns, using layers in a multiplex network to represent the mobility patterns of agents of the same class. Empirical studies on H1N1 influenza and COVID-19 can also be found in [32–37].

B. Related studies

Notably, most studies showed that travel restrictions are beneficial for suppressing a global pandemic. However, other research has yielded different results. Involving human migrations between cities, Lee *et al.* studied a modified SEIR model and found that travel restrictions are less effective for influenza epidemic control [38]. Ruan *et al.* found that, depending on the infection rate, increasing the traveling speed would result in either an enhanced or suppressed epidemic, while increasing the traveling frequency enhances the epidemic spreading [39]. During the COVID-19 pandemic, Chinazzi *et al.* indicated that sustained 90% travel restrictions to and from Mainland China only modestly affected the epidemic trajectory unless combined with a 50% or higher reduction of infection in the community [34]. Wang *et al.* used a network mean-field and gravity law of migration to establish an N-seat intertwined SIR metapopulation model. They found that migration does not directly increase epidemic replication capacity, but it can increase the influence area of an epidemic when the basic reproduction number is larger than 1 [40].

Reference [41] proposed an interregional migration model on SIR networks with distinct timescales. They obtained upper/lower bounds of the basic reproduction number $\mathcal{R}_0$ for a generic network using a perturbation approximation. Furthermore, they discovered a piecewise convergence function to the upper bound of $\mathcal{R}_0$. The above results show that more profound studies on the interregional epidemic process are required.

The spectrum of a network's Laplacian matrix can reflect its structural and dynamic properties. For example, the number of zero eigenvalues of a graph Laplacian is the number of connected components in the network. The smallest nonzero eigenvalue λ_2 of the Laplacian matrix of a network (also known as the algebraic connectivity or Fiedler value [42]) plays an important role in the dynamic process on complex networks. For instance, algebraic connectivity determines the ability of networks to synchronize, which means the larger its value, the more likely the collective behavior of nodes will emerge in the network [43]. A diffusion process refers to a phenomenon in which the nodes in a network reach a consensus. Here, the larger the algebraic connectivity, the quicker the nodes reach the same state [44]. Therefore, to investigate how network structures influence *macroscopic-level* epidemic processes, it is important to find the relation between the algebraic connectivity and the basic reproduction number.

C. Contributions of this paper

We introduce a generalized system that focuses on the migratory process between regions within a dynamic flow network context. We analyze this process using an SIR model as an example. Our contributions are as follows:

(i) We clarify the concept of an interregional migration and diffusion process. In reality, populations distribute unevenly and flow actively, not randomly, across different geographical regions. Recall that diffusion is the movement of matter or energy from a region of higher concentration to a region of lower concentration, resulting in the eventual consensus of local states [45]. The law of population conservation applies to interregional migration, meaning that the population remains constant during transportation without considering birth and death factors. This law remains valid even when the weighted flow network is imbalanced, that is, when the weighted in-degrees and out-degrees of the network are not equal. However, there are situations in which diffusion processes deviate from this law.

(ii) We devise a dynamic flow network model for investigating the macroscopic-level epidemic processes. Under the context of dynamic networks, we were able to answer the question of how network topology affects macroscopic epidemic processes. We use the same SIR model in Ref. [41] as the nodal dynamics, and the network flow instead of diffusion to describe the population flow among regions.

(iii) We study the interregional infections on SIR networks with homogeneous and heterogeneous local reproductive rates. Under the homogeneous case, we find that the speed of convergence for each region to the final equilibrium of susceptible and recovered individuals exhibits a larger variance in the ER network compared to the BA network. Considering the heterogeneous case in two special networks and a general

network, we obtain a nontrivial extension of the upper/lower bounds for $\mathcal{R}_0$ presented in Ref. [41]. We find that the local infection rates and recovery rates are independent of each other in the lower bound of $\mathcal{R}_0$, meaning the lower bound of $\mathcal{R}_0$ does not equal the mean of local basic reproduction numbers.

(iv) We establish the global asymptotic stability of the disease-free equilibrium by using the Lyapunov direct method. Based on the proof, we report a feasible way to obtain the approximated formula of $\mathcal{R}_0$ for general networks.

(v) We associate the algebraic connectivity λ_2 with $\mathcal{R}_0$ in a general formula, and we show that the increased λ_2 causes the final scale of the pandemic to *converge exponentially* to the ratio of the average local infection rate to the average local recovery rate when the local infection rates and recovery rates are heterogeneous.

(vi) Based on the general formula $\mathcal{R}_0(\lambda_2)$, we investigate the relationship between the scaling factor (coupling strength) c and $\mathcal{R}_0$. The expression of $\mathcal{R}_0(c)$ not only applies over a broader range of parameters that define its characteristics, but it also performs better than the piecewise formula around the critical value presented in [41].

(vii) We investigate the relationship between the global basic reproduction number $\mathcal{R}_0$ and other topological factors (degree distribution, average degree, network scale) that influence λ_2 of networks. We show that those factors that make λ_2 increase would help $\mathcal{R}_0$ reduce. These results provide new insight into how to control epidemiological processes from a macroscopic perspective.

(viii) Both analytical and numerical verification of the above contributions are presented.

II. MODEL FORMULATION

A. SIR-based metapopulation network model

Based on the interregional infection model in Ref. [41], we can make the following assumptions:

(i) The nodes and edges form a complex network.

(ii) Each region (e.g., a city, state, or country) can be regarded as a network node (i.e., a graph vertex).

(iii) We assume that in each region, the local population is uniformly mixed.

(iv) Population exchanges between regions can be modeled as weighted directed edges.

Next, we assume a classical SIR compartmental model upon each network node to define each region's local epidemic dynamics.

Let $\boldsymbol{x}_i(t) = (S_i(t), I_i(t), R_i(t))^T \in \mathbb{R}^3$ denote the state of region i at time t, and its components $S_i(t)$, $I_i(t)$, and $R_i(t)$ denote the number of susceptible, infected, and removed individuals in region i, respectively. For brevity, we omit the argument of each function, i.e., $\boldsymbol{x}_i$, S_i, I_i, and R_i. Without interregional migration, the nodal dynamics of region i are

$$\dot{\boldsymbol{x}}_i = f(\boldsymbol{x}_i) = \begin{bmatrix} -\beta_i \frac{I_i S_i}{N_i} \\ \beta_i \frac{I_i S_i}{N_i} - \mu_i I_i \\ \mu_i I_i \end{bmatrix}, \tag{1}$$

where $\dot{\boldsymbol{x}}_i(t)$ is the temporal derivative of $\boldsymbol{x}_i(t)$, and β_i and μ_i are the local infection and recovery rates for each region i in the network and $N_i = S_i + I_i + R_i$.

The basic reproduction number $\mathcal{R}_0^{(i)}$ of this regional model (1) defines a threshold such that if $\mathcal{R}_0^{(i)} > 1$, then the epidemic will grow in region i (assuming it is already present), whereas if $\mathcal{R}_0^{(i)} < 1$, then the epidemic will go extinct in region i. We shall call the $\mathcal{R}_0^{(i)}$'s the *local* basic reproduction numbers of the complex network. For the classical SIR compartmental model (1), we have $\mathcal{R}_0^{(i)} = \beta_i/\mu_i$ [5].

Next, we add migration dynamics to (1). Let l_{ij}, $i \neq j$, denote the migration rate of individuals from region i to region j. We thus obtain

$$\dot{\boldsymbol{x}}_i(t) = f(\boldsymbol{x}_i) + c \sum_{\substack{j=1 \\ i \neq j}}^{n} (l_{ji}\boldsymbol{x}_j - l_{ij}\boldsymbol{x}_i), \tag{2}$$

where n is the number of regions in the network, and $c > 0$ is the global coupling strength (scaling factor) that controls the overall migration rate of the network [41].

Let $\mathcal{R}_0$ denote the global basic reproduction number of the entire network. Note that $\mathcal{R}_0$ considers migrations, whereas the individual $\mathcal{R}_0^{(i)}$'s do not. In Secs. III and IV, we will compute the $\mathcal{R}_0$ of the system for various network structures and examine the roles of the network structure and human migration behavior with respect to the epidemic process.

B. Modeling physical dynamic processes on complex networks

We start by considering the importance of model selections and motivating why we chose system (2) when creating physical network models. Physical networks can have different types of flows, such as human and information flow, that can either follow or violate conservation laws [45]. On the other hand, some types of flows can move from a region of higher concentration to a lower concentration, while others can move oppositely. Therefore, it is crucial to clarify the differences among the types of flows.

1. Diffusive dynamic processes in networks

In network science, a linearly coupled dynamic process in complex dynamical networks can be written in the following form [46]:

$$\dot{\boldsymbol{x}}_i(t) = f(\boldsymbol{x}_i(t)) + c \sum_{\substack{j=1 \\ i \neq j}}^{n} l_{ij} \Gamma(\boldsymbol{x}_j(t) - \boldsymbol{x}_i(t)), \tag{3}$$

where $i = 1, \ldots, n$, $\boldsymbol{x}_i(t) = (x_{i1}(t), x_{i2}(t), \ldots, x_{im}(t))^T \in \mathbb{R}^m$ denotes the state vector of the ith node, $\dot{\boldsymbol{x}}_i(t)$ is the temporal derivative of $\boldsymbol{x}_i(t)$, and $L = (l_{ij}) \in \mathbb{R}^{n \times n}$ represents the Laplacian matrix of a general diffusive network. If the network is an undirected and unweighted graph, then L is symmetric. If the network is a directed weighted graph, then L is asymmetric. Normally, if node j receives matter/energy/information from node i, $l_{ij} \neq 0$, and $l_{ij} = 0$ otherwise, the diagonal elements are

$$l_{ii} = -\sum_{j=1, i \neq j}^{n} l_{ij}.$$

The foregoing is also known as the dissipative coupling condition. Additionally, c is the coupling strength, and $\Gamma \in \mathbb{R}^{m\times m}$ denotes the inner coupling matrix.

The advantage of Eq. (3) is that it represents a general formation of a class of problems such as the classic reaction-diffusion process, where $f(\boldsymbol{x}_i)$ represents the nodal reaction, and the Laplacian matrix denotes the diffusion among nodes. Although (3) has been widely used [20–22,25–30] to study epidemic processes in both symmetric and asymmetric networks, due to the different nature of flows, it is not appropriate for studying such processes in asymmetric networks. Therefore, the following subsection offers a general equation to deal with such kinds of network flows.

2. Dynamic processes in flow networks

When we are dealing with mobility networks among regions, i.e., interregional transportation, we can generalize the dynamics into the following form of equations:

$$\dot{\boldsymbol{x}}_i(t) = f(\boldsymbol{x}_i(t)) + c\sum_{\substack{j=1\\ i\neq j}}^{n} \Gamma(l_{ji}\boldsymbol{x}_j(t) - l_{ij}\boldsymbol{x}_i(t)). \tag{4}$$

Notably, the inner coupling matrix Γ represents the transition rates of a flow that changes its state into another during interregional transportation. To compare the difference between Eqs. (3) and (4), we first ignore nodal dynamics and inner couplings, then sum up all the subequations of system (3) and (4), respectively. If the Laplacian matrix is symmetric or balanced (in-degree equals out-degree for each node), then $\sum_{i=1}^{n} \dot{\boldsymbol{x}}_i(t) = 0$, meaning both systems follow the law of conservation. However, if the Laplacian matrix is asymmetric and imbalanced, system (3) no longer follows the law of conservation, while system (4) still does.

Furthermore, we can rewrite system (4) as

$$\dot{X} = Y - cL^T \otimes \Gamma X, \tag{5}$$

where $Y = [f(\boldsymbol{x}_1(t)), f(\boldsymbol{x}_2(t)), \ldots, f(\boldsymbol{x}_n(t))]^T$, $X = [\boldsymbol{x}_1(t), \boldsymbol{x}_2(t), \ldots, \boldsymbol{x}_n(t)]^T$, and $\otimes$ denotes the Kronecker product.

Next, consider the diffusion equation $\dot{X} = -LX$ and the interregional transportation equation $\dot{X} = -L^T X$ by ignoring nodal dynamics and inner couplings of systems (3) and (4). Note that L and L^T have the same set of eigenvalues. Assuming the Laplacian matrix of the weighted directed network (mobility network) has only one zero-eigenvalue, the final state (number of population) of X will be distributed heterogeneously according to the theory of ordinary differential equations (ODEs). When the mobility network is symmetric, X will reach a consensus under a typical diffusion process. However, when the mobility network is asymmetric and unbalanced (meaning that the in-degrees and out-degrees of the network are imbalanced), the final state of each $\boldsymbol{x}_i$ will not be the same. That is why Eq. (4) is more suitable for describing the population flow in networks than Eq. (3). Therefore, we obtain a dynamic equation capable of modeling nondiffusive physical flow systems that obey conservation laws.

3. Explicit instances of the dynamic equation

An important application of dynamic equation (4) is to describe epidemic processes with interregional transportations. For instance, in the case of an SEIR-type disease, the nodal dynamics in Eq. (4) can be substituted with a standard SEIR model equation. To study the interregional epidemic process of multivariants, one can replace $f(\boldsymbol{x}_i(t))$ with a multivariant epidemic model. In other words, depending on the research goal, the nodal dynamic in Eq. (4) can be replaced by any kind of classic epidemic model. Furthermore, the inner coupling matrix Γ makes the dynamic equation more flexible. If one wants to investigate the impact of quarantine measures and travel restrictions on the COVID-19 pandemic, one can begin by replacing the SEIHR model in the nodal dynamics of Eq. (4). After that, they can set the diagonal element linked with the isolated state or compartment of Γ to zero. One advantage of this dynamic equation is its similarity to the classic dynamic process (3). As a result, some previous research results in other domains can be directly applied to it. Notably, in this paper, we use the SIR model as an example to study the interregional epidemic process and obtain Eq. (2). Overall, there are so many potentials that remain to be explored under the dynamic equation.

III. SIR NETWORKS WITH HOMOGENEOUS LOCAL INFECTION RATES

This section considers the case in which $\beta_i = \beta$ and $\mu_i = \mu$ for all regions i in the network, as defined by (2).

A. Global basic reproduction number $\mathcal{R}_0$ of general networks

For system (2), there exists a disease-free equilibrium (DFE), namely $E^0 = [N_1^S; \ldots; N_n^S; 0; \ldots; 0]$. Since all individuals remain in the susceptible state, the number of susceptible individuals in each region, i.e., $E^S = [N_1^S; \ldots; N_n^S]$, is also the stabilized population of each region, which follows the migration dynamics

$$\dot{N}_i(t) = c\sum_{\substack{j=1\\ i\neq j}}^{n}(l_{ji}N_j - l_{ij}N_i) \quad (i = 1, \ldots, n)$$

(or $\dot{N} = -cL^T N$ in matrix form). Note that in most practical scenarios, we can assume that the populations of each region are already in stable equilibrium at $t = 0$, thus the DFE of system (2), if it exists, is simply the system's initial state, which is determined by the right eigenvector ξ of the zero-eigenvalue of L^T, with all individuals susceptible.

The DFE is stable if $\mathcal{R}_0 < 1$. To compute $\mathcal{R}_0$ for system (2), we apply the next-generation matrix method [47], producing the matrices

$$\mathcal{F} = \begin{bmatrix} \beta\frac{I_1 S_1}{N_1} \\ \vdots \\ \beta\frac{I_n S_n}{N_n} \end{bmatrix}$$

and

$$\mathcal{V} = \begin{bmatrix} \mu I_1 + c\sum_{j=1, j\neq 1}^{n}(l_{1j}I_1 - l_{j1}I_j) \\ \vdots \\ \mu I_n + c\sum_{j=1, j\neq n}^{n}(l_{nj}I_1 - l_{jn}I_j) \end{bmatrix}.$$

From $\mathcal{F}$ and $\mathcal{V}$, and linearizing about the DFE E^0, we obtain the Jacobian matrices $F = \beta\mathbf{I}$ and $V = cL^T + \mu\mathbf{I}$, where $\mathbf{I}$ is the identity matrix.

The value $\mathcal{R}_0$ is the spectral radius (maximum of the absolute values of the eigenvalues) of FV^{-1}. However, V^{-1} is difficult to compute. Instead, we note that the eigenvalues of FV^{-1} are reciprocals of those of $VF^{-1} = V/\beta$. Since $V = cL^T + \mu\mathbf{I}$, the smallest eigenvalue of V is μ. Therefore, the smallest eigenvalue of VF^{-1} is μ/β. We thus obtain the following:

Theorem 1. The global basic reproduction number $\mathcal{R}_0$ of the SIR network is β/μ, independent of the Laplacian matrix L. In other words, $\mathcal{R}_0$ is independent of network migration when all the local infection and recovery rates are homogeneous across regions, becoming simply the ratio between the global infection and recovery rates.

B. Numerical results

In this subsection, we consider the evolution of system (2) on random and scale-free networks, namely Erdős-Rényi (ER) [10], Barabási-Albert (BA) [12], and Watts-Strogatz (WS) [11] networks. Figure 1 shows the evolution of (2) for a 100-region ER network and a 100-region BA network, with $N_i = 10^6$ individuals in each region. The network parameters of the ER model are $p = 1$ (probability that an edge is rewired in the network), and that of the BA model are $m_0 = 3$ (number of initial nodes) and $m = 2$ (new edges per added node). The average degree of both networks is $\langle k\rangle = 2$.

We define $\beta = 0.25$, $\mu = 0.1$, and $l_{ij} = 0.001$ for all regions i and $j \neq i$. In other words, $\mathcal{R}_0 = 2.5$, via Theorem 1. The initial state of the network is such that there is a single infected individual in some randomly chosen region of the network, to which all other individuals are susceptible.

As the final proportion of recovered individuals depends solely on $\mathcal{R}_0$, we find that all trajectories in both panels of Fig. 1 converge to the same value. However, the speed of convergence for each region to the final equilibrium of susceptible and recovered individuals exhibits a larger variance in the ER case compared to the BA case.

Figure 2 considers a 100-region WS network with average degree $\langle k\rangle = 2$ (again with $N_i = 10^6$ individuals in each region and $\beta = 0.25$, $\mu = 0.1$, and $l_{ij} = 0.001$ for all regions i and $j \neq i$), and it shows the final proportion of recovered individuals with respect to the rewiring probability of the WS network. Note that a rewiring probability of 0 yields a k-regular ring lattice, while a rewiring probability of 1 yields an ER random network. It is demonstrated that the final proportion of recovered individuals is not sensitive to the rewiring probability of the WS network. This is consistent with Theorem 1.

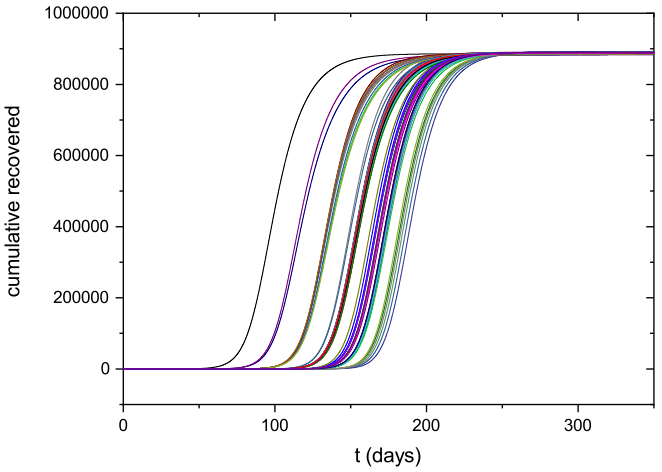

(a) ER network

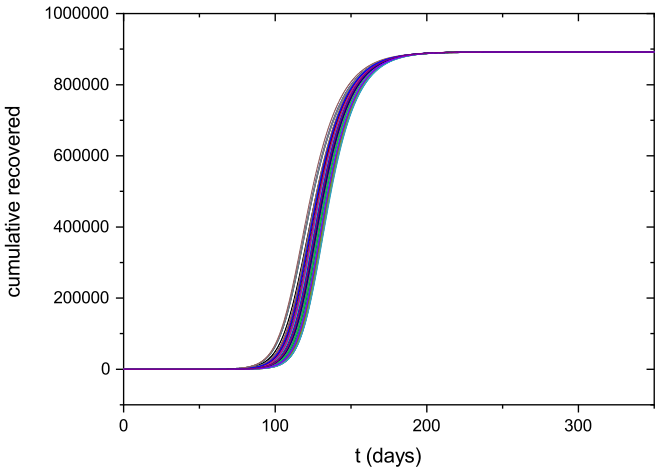

(b) BA network

FIG. 1. Cumulative recovered individuals in a 100-region SIR network with homogeneous infection and recovery rates. Each line represents one of the regions.

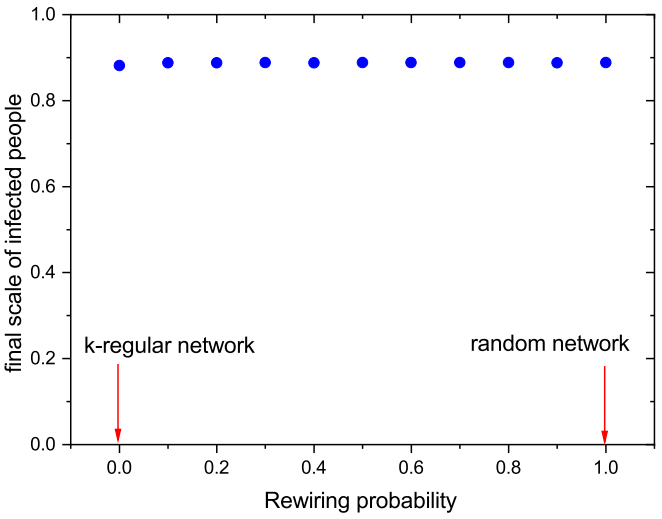

FIG. 2. Final proportion of recovered individuals in a 100-region SIR WS network with homogeneous infection and recovery rates, where $\beta = 0.25$ and $\mu = 0.1$ (average of 20 network instances).

IV. SIR NETWORKS WITH HETEROGENEOUS LOCAL INFECTION RATES AND RECOVERY RATES

In Sec. III, we considered the case in which all regions' disease infection rates are equal. However, this is not applicable to most real-world systems, due to differences in population densities, climate, government policies, etc., which lead to differences in regional infection rates. In this section, we consider different values of the local infection rates β_i in the network along with different values of local recovery rates μ_i.

A. Upper and lower bounds of $\mathcal{R}_0$ in two kinds of network

Applying the next-generation matrix method, we find that $\mathcal{R}_0$ is the smallest eigenvalue of the matrix $M = VF^{-1}$, where $V = [L^T + \text{diag}(\mu_1, \ldots, \mu_n)]$ and $F = \text{diag}(\beta_1, \beta_2, \ldots, \beta_n)$. In other words,

$$M = [L^T + \text{diag}(\mu_1, \ldots, \mu_n)]\text{diag}(1/\beta_1, \ldots, 1/\beta_n).$$

However, since the eigenvalues of M are difficult to find in the general case, below we will focus on two special cases: a fully connected network and a star network.

1. Fully connected network

We consider a fully connected network with equal migration rates on all edges, such that $l_{ij} = c$ for all $i \neq j$. Thus, the Laplacian matrix L is

$$L = c(n\mathbf{I} - \mathbf{J}),$$

where $\mathbf{J}$ is a matrix of 1's. Then we can have the following theorem:

Theorem 2. Considering a fully connected undirected SIR network with heterogeneous local infection rates and recovery rates, if the coupling strength is large enough, the global basic reproduction number will converge to $\mathcal{R}_0 = \bar{\beta}/\bar{\mu}$, where $\bar{\beta}$ and $\bar{\mu}$ are the mean of nodal infection rates and recovery rate, respectively.

Similarly, the following corollary can be obtained:

Corollary 1. Considering a fully connected undirected SIR network with heterogeneous local infection rates and recovery rates, if the coupling strength is small enough, the global basic reproduction number $\mathcal{R}_0$ will get close to the largest nodal basic reproduction number, $\max_i \beta_i/\mu_i$.

The proof can be found in Appendix A.

2. Star network

We consider a star network with equal migration rates on all edges, such that $l_{i,j} = c$ for all $i \neq j$. We define region 1 to be the hub of the network, i.e., the Laplacian matrix is

$$L = c\begin{bmatrix} n-1 & -1 & \cdots & -1 \\ -1 & 1 & & \\ \vdots & & \ddots & \\ -1 & & & 1 \end{bmatrix}.$$

We summarize our findings as follows:

Theorem 3. Considering a star undirected SIR network with heterogeneous local infection rates and recovery rates, if the coupling strength is large enough, the global basic reproduction number will converge to $\mathcal{R}_0 = \bar{\beta}/\bar{\mu}$, where $\bar{\beta}$ and $\bar{\mu}$ are the mean of nodal infection rates and recovery rate, respectively.

Corollary 2. Considering a star undirected SIR network with heterogeneous local infection rates and recovery rates, if the coupling strength is small enough, the global basic reproduction number $\mathcal{R}_0$ will get close to the largest nodal basic reproduction number, $\max_i \beta_i/\mu_i$.

The proof can be found in Appendix B.

It is obvious that if one keeps increasing the connectivity of a network, that network will eventually become a fully connected one. That means the spectrum property of their M matrices will converge as the connectivity increases. Therefore, we have the following statements:

Remark 1. High connectivity for an SIR network with heterogeneous local reproductive rates means its global basic reproduction number will get close to the ratio of the average local infection rate to the average local recovery rate.

There are many methods to increase the connectivity of one network, for example, increasing the average degree, i.e., adding more links to the network, shortening the average shortest path length, or reducing the network scale. In the next section, we will validate the above statements both analytically and numerically.

B. Lyapunov stability of the disease-free equilibrium of general networks

The latest section shows that obtaining analytical results of $\mathcal{R}_0$ for general network structure is very challenging. Therefore, this section uses Lyapunov stability analysis to find $\mathcal{R}_0$ for more general cases. To estimate the $\mathcal{R}_0$ of system (2), we need to find the stability condition of the DFE $E^0 = [N_1^S; \ldots; N_n^S; 0; \ldots; 0]$. We shall prove the disease-free equilibrium's global stability by means of Lyapunov's second method.

Theorem 4. Consider system (2). The disease-free equilibrium $E^0 = [N_1^S; \ldots; N_n^S; 0; \ldots; 0]$ of (2) is globally asymptotically stable if $\mathcal{R}_0 < 1$, where $\mathcal{R}_0 = \bar{\beta}/\bar{\mu} + g$, and g is a parameter function that belongs to a bounded set associated with the network.

The proof can be found in Appendix C.

Remark 2. Theorem 4 implies that $\mathcal{R}_0 = \bar{\beta}/\bar{\mu} + g$ is an analytical formula for the global basic reproduction number. By using a numerical approximation, we are able to determine a more accurate form of g.

Next, we set out to obtain an approximation of g. In the following section, we will determine the relationship between g and the network structure using numerical methods.

C. Numerical results about $\mathcal{R}_0$ in general networks

In this section, we investigate the relationship between the macroscopic-level epidemic process and the network topology. We compute $\mathcal{R}_0$ of some representative networks. We shall assign initial populations $N_i = 10^6$ and infection rates $\beta_i \sim$ normal ($u = 0.125, \sigma^2 = 0.1$) for each of the n regions, and a global recovery rate of $\mu = 0.1$, except for Figs. 3 and 5.

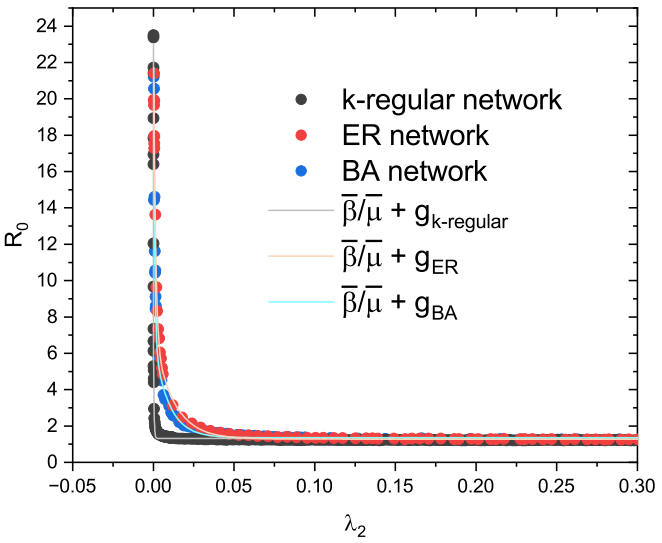

FIG. 3. $\mathcal{R}_0$ with respect to λ_2 on different kinds of SIR networks with heterogeneous local infection rates $\beta_i \sim \text{normal}(u = 0.125, \sigma^2 = 0.1)$ and recovery rates $\mu_i \sim \text{normal}(u = 0.1, \sigma^2 = 0.05)$ (average of 100 network instances).

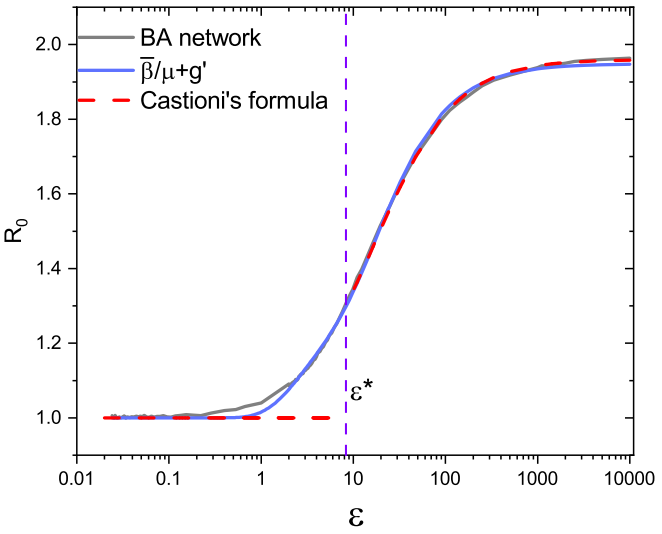

FIG. 5. $\mathcal{R}_0$ with respect to ε on Barabási-Albert (BA) SIR network with heterogeneous local infection rates $\beta_i \sim \text{normal}(u = 0.125, \sigma^2 = 0.1)$ and homogeneous recovery rates $\mu = 0.125$ (average of 100 network instances). The critical value $\varepsilon^* = 1/(\beta_{\max} - \mu)$.

1. A general formula for $\mathcal{R}_0$

In general, we can directly calculate $\mathcal{R}_0$ from the matrix M; however, we still need to know the relationships between $\mathcal{R}_0$ and various parameters, such as local infection rate β_i, local recovery rate μ_i, and other parameters associated with the network topology. Those kinds of relations cannot be directly obtained from matrix M. Theorem 4 provides a rough approximation of $\mathcal{R}_0$. By introducing the algebraic connectivity λ_2 as a parameter of $\mathcal{R}_0$, we are able to associate the macroscopic-level epidemic process and the network topology. It is worth noting that λ_2 is generally considered as a function of the network structure's directly associated parameters, such as scaling factor (coupling strength), average degree, network scale, and so on. There is no universal formula for calculating λ_2 that applies to all networks. However, it is possible to derive approximated formulas for λ_2 for specific types of networks [48,49].

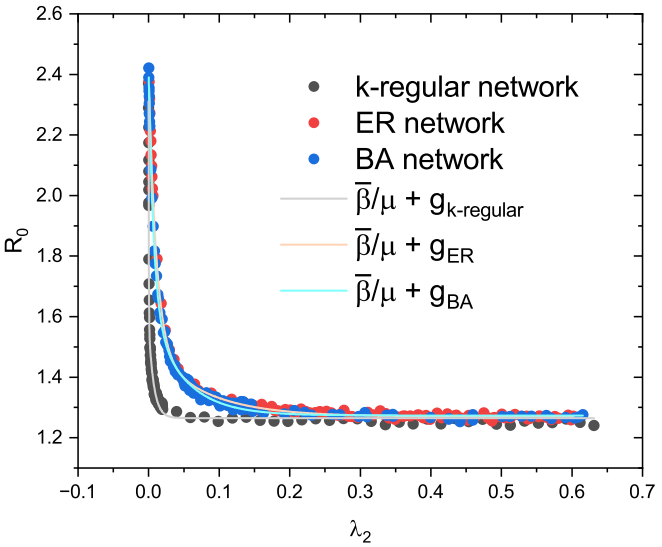

FIG. 4. $\mathcal{R}_0$ with respect to λ_2 on different kinds of SIR networks with heterogeneous local infection rates $\beta_i \sim \text{normal}(u = 0.125, \sigma^2 = 0.1)$ and homogeneous recovery rates $\mu = 0.1$ (average of 100 network instances).

Figure 3 shows the global basic reproduction number calculated by the next-generation matrix method under different kinds of SIR networks with heterogeneous local infection rates and recovery rates (colored dots). It is demonstrated that $\mathcal{R}_0$ decays as λ_2 increases. The numerical results suggest that $\mathcal{R}_0$ follows an exponential decay rule with respect to λ_2, i.e., $g = A_1 e^{-h_1\lambda_2} + A_2 e^{-h_2\lambda_2}$, where A_1, A_2, h_1, and h_2 are tunable parameters. Therefore, an analytical formula for the basic reproduction number is obtained,

$$\mathcal{R}_0(\lambda_2) = \bar{\beta}/\bar{\mu} + A_1 e^{-h_1\lambda_2} + A_2 e^{-h_2\lambda_2}. \tag{6}$$

The solid lines in Fig. 3 represent the fitted values of $\mathcal{R}_0$ according to (6). The fitted lines agree closely with the empirical data, demonstrating the veracity of the exponential fit.

Figure 4 shows the global basic reproduction number of different kinds of SIR networks with heterogeneous local infection rates and homogeneous recovery rates μ. Not surprisingly, the trends of Figs. 3 and 4 are almost identical. Notably, Fig. 3 has a larger drop due to the large difference between $\max_i \beta_i/\mu_i$ and $\bar{\beta}/\bar{\mu}$. Therefore, for simplicity, we consider homogeneous μ in the following simulations.

2. Increasing scaling factor reduces $\mathcal{R}_0$

The global coupling strength c is a scaling factor of the Laplacian matrix, which has a linear relationship with the eigenvalues of L. Therefore, we postulate that $g'(c) = A_1 e^{-h_1' c} + A_2 e^{-h_2' c}$. Reference [41] derives the relationship of $\mathcal{R}_0$ and a scaling factor ε. To compare the formula $\mathcal{R}_0(c) = \bar{\beta}/\bar{\mu} + g'(c)$ with Castioni's $\mathcal{R}(\varepsilon)$ [41], we rewrite

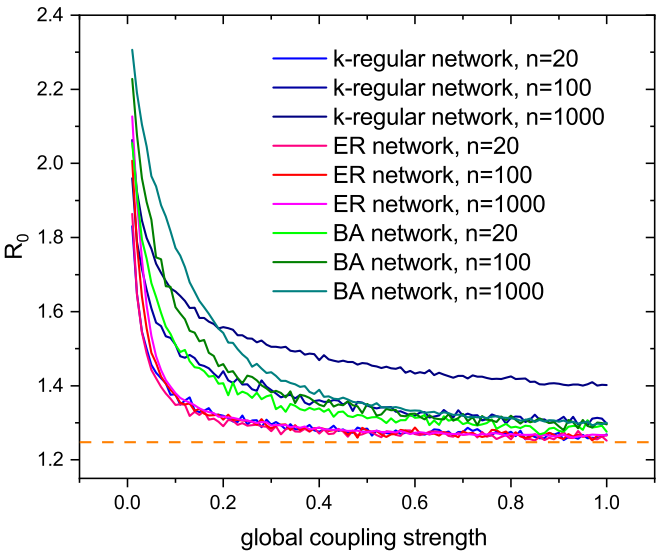

FIG. 6. Interregional infection on different kinds of SIR networks with an average degree $\langle k\rangle = 4$, with heterogeneous local infection rates $\beta_i \sim \text{normal}(u = 0.125, \sigma^2 = 0.1)$ and homogeneous recovery rates $\mu = 0.1$ (average of 100 network instances).

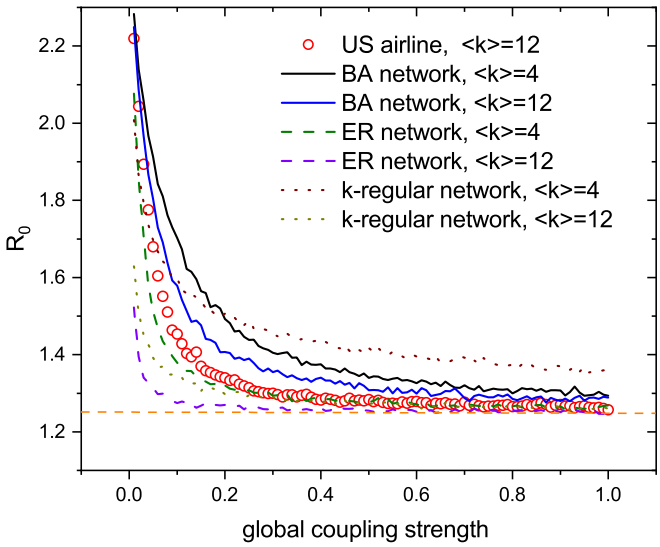

FIG. 7. Interregional infection on the U.S. airline network and synthetic networks with $n = 332$ nodes, with local infection rates $\beta_i \sim \text{normal}(u = 0.125, \sigma^2 = 0.1)$ and homogeneous recovery rates $\mu = 0.1$ (average of 100 network instances).

$g'(c)$ into $f(\varepsilon) = A_1 e^{-h_1'/\varepsilon} + A_2 e^{-h_2'/\varepsilon}$ based on $c = 1/\varepsilon$. Figure 5 shows both Castioni's formula and ours, with the latter applying over a broader range of parameters to define its characteristics, and it performs better than Castioni's piecewise formula around the critical value $\varepsilon^* = 1/(\beta_{\max} - \mu)$.

Figure 6 shows the global basic reproduction number for different kinds of SIR networks with heterogeneous local infection rates with the same average degree $\langle k\rangle = 4$. Surprisingly, regardless of the network type and network scale, all the R_0's will reduce to $\bar{\beta}/\mu$ (orange dashed line) when the global coupling strength increases. Such convergence is aligned with the analytical results in Sec. IV A. Because of the linear relationship between λ_2 and the global coupling strength, the results are also aligned with the formula (6). Furthermore, the rates of such convergence are quite different for different networks. The R_0 reduction on regular networks is much slower than on other randomized networks. This is because those regular networks have a much larger average shortest path length, which means they have poor connectivity and are located far from the baseline, the fully connected network. These results suggest that increasing human traffic flow on interregional networks can reduce the global spreading speed of an epidemic process.

Figure 7 explores the above-mentioned phenomena on synthetic and real-world networks. The red circles represent the calculated R_0 based on a U.S. airline network (1997) comprising 332 nodes (cities) and 12 average edges (airlines) for each node [50]. The other lines represent different synthetic networks consisting of 332 nodes. Considering the same average degree $\langle k\rangle = 12$, the airline network's epidemiological performance is similar to that of a BA network. This is simply because the airline network's degree distribution is similar to that of BA networks.

To relate the computed $\mathcal{R}_0$ values to the *final* cumulative proportion of infected individuals, Fig. 8 plots this proportion with respect to c for a U.S. airline network, regular, ER, and BA networks with $n = 332$ nodes and an average degree of $\langle k\rangle = 12$. Gray bands denote the 5th and 95th percentiles for 20 network instances, as simulated using the Runge-Kutta method, whereas the solid line denotes the mean. Consistent with Fig. 7, this proportion decreases with c. Additionally, we plot the arrival time of the peak of infected people in Fig. 9. Surprisingly, the epidemic peak time increases as the global coupling strength increases. In other words, the increase in the migration rate can reduce the final epidemic scale and postpone the epidemic peak.

3. Increasing average node degree reduces $\mathcal{R}_0$

The above results also show that networks with a larger average degree exhibit better performance for reducing the R_0. For those who have small average degrees, their R_0's are much higher than the averaged nodal R_0^i, especially when the coupling is weak. This is because the larger the average degree is, the closer the graph will be to a complete graph. In other words, the λ_2 will reach its maxima if we keep inserting links to the network. According to Eq. (6), as λ_2 increases, R_0 will reduce an approach to the lower bound.

We consider a k-regular network, an ER network, and a BA network with $n = 100$ regions, where the global coupling strength $c = 0.1$. Figure 10 shows the computed $\mathcal{R}_0$ value with respect to the average degree $\langle k\rangle$. It is demonstrated that while $\mathcal{R}_0$ converges to $\bar{\beta}/\mu$ when $\langle k\rangle$ is high, BA networks produce the highest $\mathcal{R}_0$ out of the three network types when the migration rate is low, which aligns with the finding in Fig. 6. As in the previous example, a higher mean node degree leads to a lower average path length, and therefore a lower cumulative number of infections.

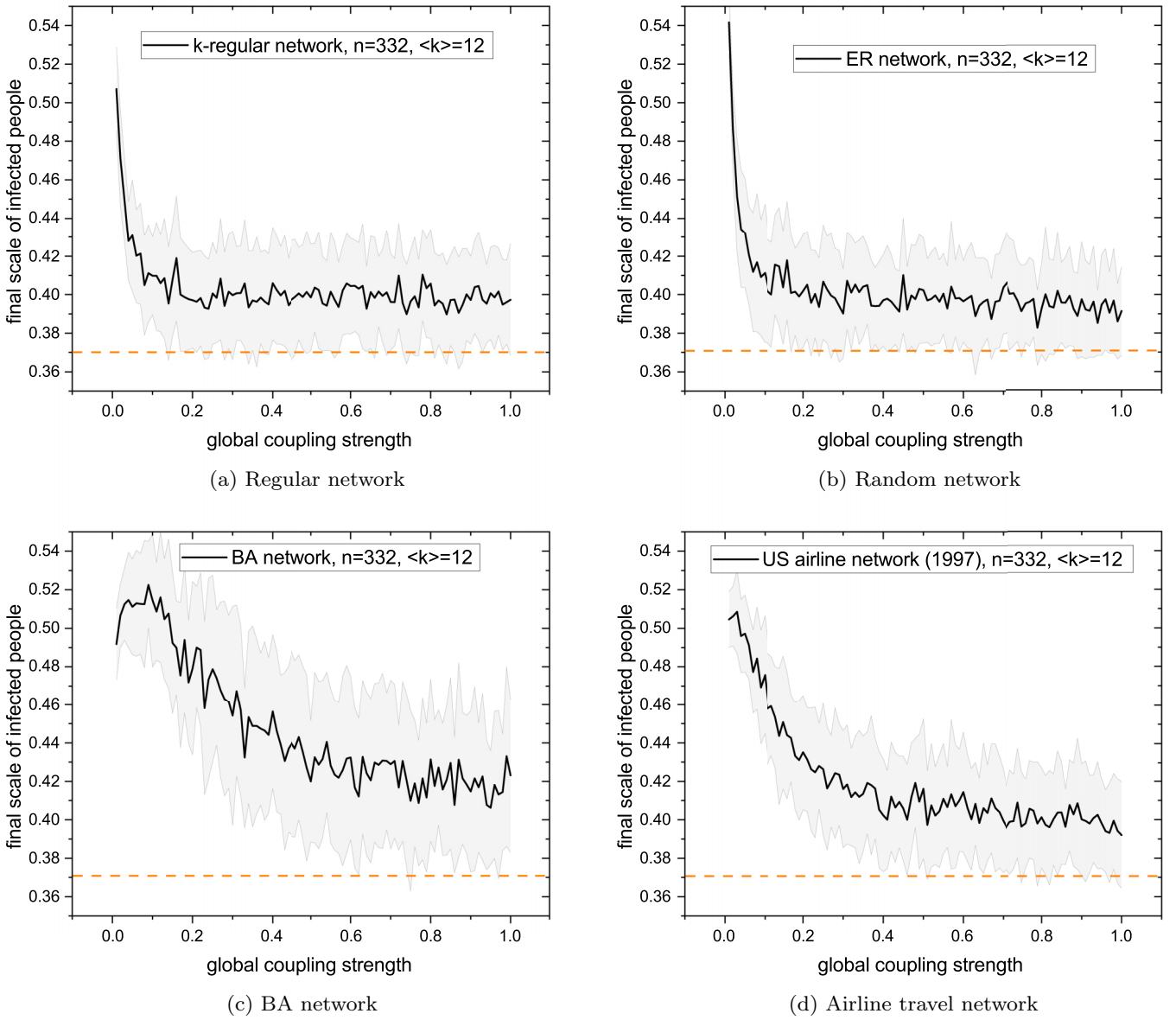

(a) Regular network (b) Random network

(c) BA network (d) Airline travel network

FIG. 8. Final scale of interregional pandemics on SIR networks with $n = 332$ nodes and an average degree of $\langle k \rangle = 12$, with local infection rates $\beta_i \sim \text{normal}(u = 0.125, \sigma^2 = 0.1)$ and homogeneous recovery rates $\mu = 0.1$. The solid black line represents the average data from 30 network instances, with the shaded area indicating the margin of error for each data point. The orange dashed line represents the expected final epidemic scale of the classic SIR model with $\mathcal{R}_0 = 1.25$.

4. Reducing network size reduces $\mathcal{R}_0$

In Fig. 11, we consider $\mathcal{R}_0$ with respect to the network size for a BA network and three WS networks with rewiring probabilities of 0, 0.1, and 1. Note that $p = 0$ yields a regular ring lattice while $p = 1$ approximates an ER random network. Note that for large network sizes, $\mathcal{R}_0$ is approximately linear in n, the network size, whereas for low values of p, $\mathcal{R}_0$ continues to increase with n even for thousands of network nodes. To explain this, note that the average path length in ER and BA networks experiences a saturation effect for large network sizes [51], whereas for a ring lattice, the average path length is approximately linear in n. Reference [48] shows that for BA networks, λ_2 remains constant as the network scale (size) enlarges. As for k-regular and WS networks, λ_2 decreases as n increases [49].

After analyzing the above results, it can be concluded that curves for k-regular networks are always higher than those of ER networks. This is because the value of λ_2 is always higher for ER networks as compared to k-regular networks when they have the same parameter settings.

V. DISCUSSION AND FUTURE WORKS

This paper introduced an SIR-based interregional epidemic model on complex networks, with the population divided

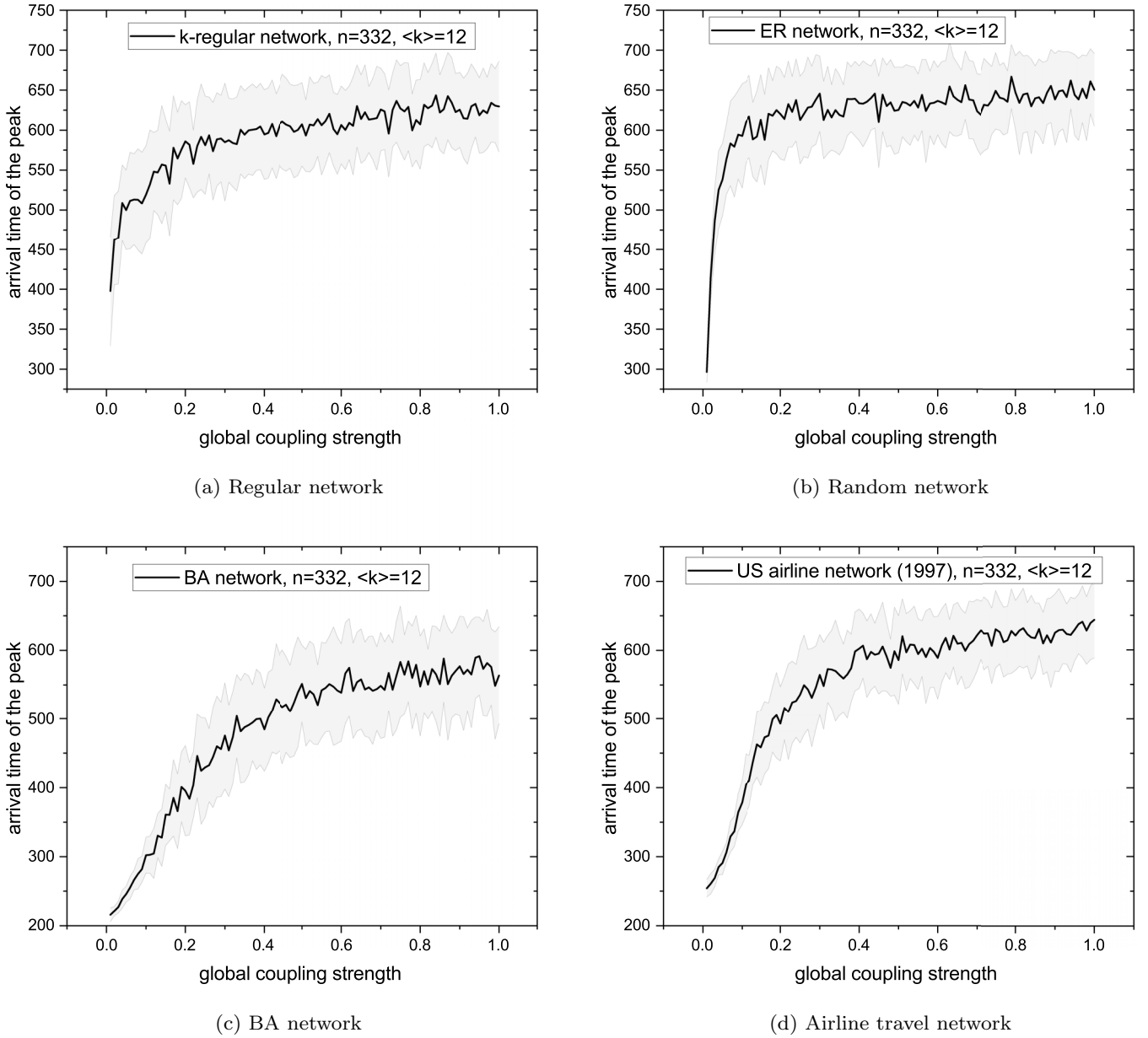

(a) Regular network

(b) Random network

(c) BA network

(d) Airline travel network

FIG. 9. Arrival time (the date since the first case) of the epidemical peak of interregional pandemics on SIR networks with $n = 332$ nodes and an average degree of $\langle k \rangle = 12$, with local infection rates $\beta_i \sim \text{normal}(u = 0.125, \sigma^2 = 0.1)$ and homogeneous recovery rates $\mu = 0.1$. The solid black line represents the average data from 30 network instances, with the shaded area indicating the margin of error for each data point.

into regions with migration between them. The model can be expressed as the combination of local epidemic dynamics and interregion migration dynamics, which are defined by a general dynamic equation using the transpose of the Laplacian matrix [see (5)].

Note that the presence of the diagonal inner coupling matrix in (5) reflects the fact that all individuals in the model are allowed to migrate between regions without restriction. We can replace this with a more general inner coupling matrix to represent different cases. For example, if all infected individuals are barred from traveling between regions, the corresponding diagonal entry will become zero. If people can become infected during interregional migration, the nondiagonal entry will become nonzero. A more realistic model may instead differentiate between known and unknown (latent or asymptomatic) infections, thus adding more compartments to the epidemic model.

An interesting result of epidemic networks, such as the one proposed in this paper, is that increasing the network's algebraic connectivity by manipulating the network topology (degree distribution, average degree, network size, scaling factor, etc.) can lead to a lower number of cumulative infections and a later epidemic peak, as shown in Secs. III and IV. Previously, in [41,52], scientists reported similar phenomena by changing the global scaling factor. In other words, a tradeoff may exist between reducing global infections and

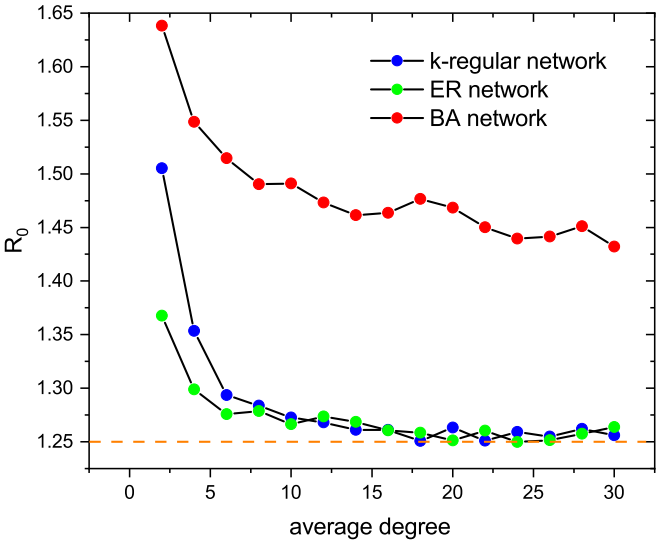

FIG. 10. $\mathcal{R}_0$ with respect to average degree on different kinds of SIR networks with $n = 100$ regions, with the global coupling strength $c = 0.1$, local infection rates $\beta_i \sim \text{normal}(u = 0.125, \sigma^2 = 0.1)$, and homogeneous recovery rates $\mu = 0.1$ (average of 100 network instances).

maintaining the stability of local health systems, which may collapse if an epidemic happens too quickly. Furthermore, although travel restrictions may delay the onset of an epidemic locally, they are ineffective in the long-term [53]. Ideally, policymakers will continuously adjust travel policies according to the global situation, in combination with interventions to limit local spreading. The impact of travel restrictions on the economy and public well-being should also be considered [54].

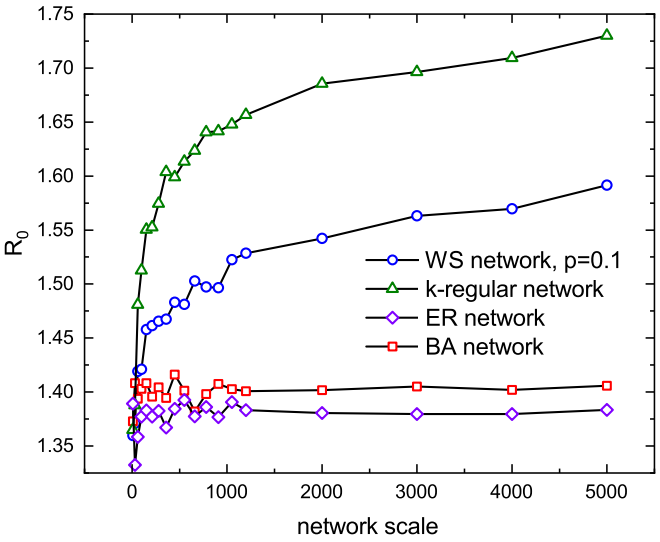

FIG. 11. $\mathcal{R}_0$ with respect to network scale on different kinds of SIR networks with an average degree $\langle k \rangle = 4$, with the global coupling strength $c = 0.1$, local infection rates $\beta_i \sim \text{normal}(u = 0.125, \sigma^2 = 0.1)$, and homogeneous recovery rates $\mu = 0.1$ (average of 100 network instances).

In general, the next-generation matrix method can directly calculate $\mathcal{R}_0$ from the matrix M. However, we still need to know the relationships between $\mathcal{R}_0$ and various parameters, such as local infection rate β_i, local recovery rate μ_i, and particularly parameters associated with the network topology. The above shows the potential value of formula (6) when we are dealing with real mobility networks when having only limited knowledge of the graph. If we can estimate the algebraic connectivity of a class of networks [48,49], we may be able to obtain $\mathcal{R}_0$ without complete knowledge of the mobility network. This will be extremely useful and important for preventing future global pandemics.

Our dynamic equation exhibits great potential that can be applied to many kinds of infectious diseases. In the future, we will introduce multivariant dynamics, the SEIHR model [7,8], and the SVEIHR model [9] into the dynamic equation and discover more interesting phenomena. Furthermore, we will use a more general epidemic model to verify the current paper's results. By uncovering universalities that underpin epidemic processes with interregional migration, we will contribute significantly to this area of research.

Although this paper provides interesting results for several network types, it contains several limitations. First, our theoretical results do not explicitly express g. Second, other kinds of epidemic models remain to be studied. Further research is required to examine network dynamics on more general networks. Finally, the effect of time-varying migration controls, e.g., in response to disease incidence in adjacent regions, also needs further research.

VI. CONCLUDING REMARKS

This paper investigated an SIR model for interregional epidemic infection in complex networks. The model considered geographically distributed populations as interconnected nodes and described the interregional transportation of a network using a generalized formula that extended the classic dynamical complex network systems. The paper studied interregional infection on SIR networks with homogeneous local reproduction rates and derived the global basic reproduction number ($\mathcal{R}_0$) using the next-generation matrix method. The results showed that travel restrictions may not influence the final epidemic scale in the whole system as long as the regions are interconnected. Interregional infection on SIR networks with heterogeneous local infection rates and recovery rates was explored, and the analytical results of the global basic reproduction number on fully connected networks and star networks were obtained. The results suggest that increasing network connectivity can make the global spreading speed converge to the ratio of the average local infection rate to the average local recovery rate. By using the second Lyapunov method, more general results are obtained, which support the results derived from the next-generation matrix method. Further investigations show that the rate of convergence is exponential with respect to the second smallest Laplacian eigenvalue. Numerical results on real-world and synthetic networks also suggest that increasing the migration rate can lead to fewer cumulative infections and a later epidemic peak. The study revealed interesting results about the effectiveness of travel restrictions, and it highlights the need for

policymakers to consider the tradeoffs between the final global epidemic scale and arrival times of the local peak. The proposed model's limitations include being based on a SIR model and not verifying if other models, such as SIRS and SEIR, have the same properties discovered. Analytical results for more general networks also remain unresolved. Overall, the proposed model covers a wide range of research questions and provides insights into interregional epidemic infection in complex networks.

ACKNOWLEDGMENTS

This work was supported by the National Natural Science Foundation of China (Grant No. 62006159), the Health and Medical Research Fund of Hong Kong (16171921), and the Research Grants Council (RGC) of Hong Kong under General Research Fund (Grants No. 11104620, No. 11102421, and No. 11101422).

All the authors declare that they have no conflict of interest.

APPENDIX A: PROOF OF THEOREM 2 AND COROLLARY 1

Proof. The characteristic polynomial of a fully connected network's $M = [L^T + \mathrm{diag}(\mu_1, \ldots, \mu_n)]\mathrm{diag}(1/\beta_1, \ldots, 1/\beta_n)$ is

$$P = \det(M - \hat{\lambda}\mathbf{I}) = \det\begin{bmatrix} \frac{\mu_1+(n-1)c}{\beta_1} - \hat{\lambda} & -\frac{c}{\beta_2} & \cdots & -\frac{c}{\beta_n} \\ -\frac{c}{\beta_1} & \frac{\mu_2+(n-1)c}{\beta_2} - \hat{\lambda} & \cdots & -\frac{c}{\beta_n} \\ \vdots & \vdots & \ddots & \vdots \\ -\frac{c}{\beta_1} & -\frac{c}{\beta_2} & \cdots & \frac{\mu_n+(n-1)c}{\beta_n} - \hat{\lambda} \end{bmatrix}.$$

Applying the row operation $\boldsymbol{r}_1 \leftarrow \sum_{i=1}^{n} \boldsymbol{r}_i$, we obtain

$$P = \det\begin{bmatrix} \frac{\mu_1}{\beta_1} - \hat{\lambda} & \frac{\mu_2}{\beta_2} - \hat{\lambda} & \cdots & \frac{\mu_n}{\beta_n} - \hat{\lambda} \\ -\frac{c}{\beta_1} & \frac{\mu_2+(n-1)c}{\beta_2} - \hat{\lambda} & \cdots & -\frac{c}{\beta_n} \\ \vdots & \vdots & \ddots & \vdots \\ -\frac{c}{\beta_1} & -\frac{c}{\beta_2} & \cdots & \frac{\mu_n+(n-1)c}{\beta_n} - \hat{\lambda} \end{bmatrix}.$$

Applying the column operations $\boldsymbol{c}_j \leftarrow \boldsymbol{c}_j - \boldsymbol{c}_1\beta_1/\beta_j$, $j = 2, \ldots, n$, we obtain

$$P = \det\begin{bmatrix} \frac{\mu_1}{\beta_1} - \hat{\lambda} & \left(\frac{\mu_2-\mu_1+\beta_1\hat{\lambda}}{\beta_2}\right) - \hat{\lambda} & \cdots & \left(\frac{\mu_n-\mu_1+\beta_1\hat{\lambda}}{\beta_n}\right) - \hat{\lambda} \\ -\frac{c}{\beta_1} & \frac{\mu_2+nc}{\beta_2} - \hat{\lambda} & \cdots & 0 \\ \vdots & \vdots & \ddots & \vdots \\ -\frac{c}{\beta_1} & 0 & \cdots & \frac{\mu_n+nc}{\beta_n} - \hat{\lambda} \end{bmatrix}.$$

Finally, applying the row operation

$$\boldsymbol{r}_1 \leftarrow \boldsymbol{r}_1 - \sum_{i=2}^{n} \boldsymbol{r}_i \frac{(\mu_i - \mu_1) + (\beta_1 - \beta_i)\hat{\lambda}}{\mu_i - \mu_1 - \beta_i\hat{\lambda}},$$

we obtain

$$P = \det\begin{bmatrix} \beta_1\Lambda & 0 & \cdots & 0 \\ -\frac{c}{\beta_1} & \frac{\mu_2+nc}{\beta_2} - \hat{\lambda} & \cdots & 0 \\ \vdots & \vdots & \ddots & \vdots \\ -\frac{c}{\beta_1} & 0 & \cdots & \frac{\mu_n+nc}{\beta_n} - \hat{\lambda} \end{bmatrix},$$

where

$$\beta_1\Lambda = \mu_1 - \hat{\lambda}\beta_1 + c\sum_{i=2}^{n} \frac{(\mu_i - \mu_1) + (\beta_1 - \beta_i)\hat{\lambda}}{\mu_i - \mu_1 - \beta_i\hat{\lambda}}.$$

Since we now have a triangular matrix,

$$P = \beta_1\Lambda \prod_{i=2}^{n} \left(\frac{\mu_i + nc}{\beta_i} - \hat{\lambda}\right).$$

The eigenvalues of M are the zeros of P and are thus $\{\hat{\lambda}_1, \ldots, \hat{\lambda}_n\}$, where $\hat{\lambda}_1$ is the solution to $(\beta_1\Lambda = 0)$ and $\hat{\lambda}_i = (\mu_i + nc)/\beta_i$ for $i = 2, \ldots, n$. Finally, $\mathcal{R}_0 = 1/\min_i \hat{\lambda}_i$.

When $c \to \infty$, we have

$$\begin{aligned} \beta_1\Lambda &\to \mu_1 - \hat{\lambda}\beta_1 - \sum_{i=2}^{n} \frac{(\mu_i - \mu_1) + (\beta_i - \beta_1)\hat{\lambda}}{n} \\ &= \frac{1}{n}\sum_{i=1}^{n} \mu_i - \frac{\hat{\lambda}}{n}\sum_{i=1}^{n} \beta_i. \end{aligned}$$

Thus, $\hat{\lambda}_1 \to \bar{\mu}/\bar{\beta}$, where $\bar{\beta}$ and $\bar{\mu}$ are the mean of all the regions' local infection rates and recovery rates, respectively. Furthermore, $\hat{\lambda}_i \to \infty$ for all $i \neq 1$. Therefore, $\mathcal{R}_0 \approx \bar{\beta}/\bar{\mu}$. When $c \to 0$, $\hat{\lambda}_i \to \mu_i/\beta_i$ for all $i = 1, \ldots, n$, and $\mathcal{R}_0 \approx \max_i \beta_i/\mu_i$, i.e., the maximum basic reproduction number of the isolated regions.

APPENDIX B: PROOF OF THEOREM 3 AND COROLLARY 2

Proof. The characteristic polynomial of a star network's $M = [L^T + \mathrm{diag}(\mu_1, \ldots, \mu_n)]\mathrm{diag}(1/\beta_1, \ldots, 1/\beta_n)$ is

$$P = \det(M - \hat{\lambda}\mathbf{I}) = \det\begin{bmatrix} \frac{\mu_1+(n-1)c}{\beta_1} - \hat{\lambda} & -\frac{c}{\beta_2} & \cdots & -\frac{c}{\beta_n} \\ -\frac{c}{\beta_1} & \frac{\mu_2+c}{\beta_2} - \hat{\lambda} & \cdots & 0 \\ \vdots & \vdots & \ddots & \vdots \\ -\frac{c}{\beta_1} & 0 & \cdots & \frac{\mu_n+c}{\beta_n} - \hat{\lambda} \end{bmatrix}.$$

Applying the row operation $\boldsymbol{r}_1 \leftarrow \sum_{i=1}^n \boldsymbol{r}_i$, we obtain

$$P = \det\begin{bmatrix} \frac{\mu_1}{\beta_1} - \hat{\lambda} & \frac{\mu_2}{\beta_2} - \hat{\lambda} & \cdots & \frac{\mu_n}{\beta_n} - \hat{\lambda} \\ -\frac{c}{\beta_1} & \frac{\mu_2+c}{\beta_2} - \hat{\lambda} & \cdots & 0 \\ \vdots & \vdots & \ddots & \vdots \\ -\frac{c}{\beta_1} & 0 & \cdots & \frac{\mu_n+c}{\beta_n} - \hat{\lambda} \end{bmatrix}.$$

Then, applying the row operation

$$\boldsymbol{r}_1 \leftarrow \boldsymbol{r}_1 - \sum_{i=2}^n \boldsymbol{r}_i \frac{\mu_i - \beta_i\hat{\lambda}}{\mu_i + c - \beta_i\hat{\lambda}},$$

we obtain

$$P = \det\begin{bmatrix} \beta_1\Lambda & 0 & \cdots & 0 \\ -\frac{c}{\beta_1} & \frac{\mu_2+c}{\beta_2} - \hat{\lambda} & \cdots & 0 \\ \vdots & \vdots & \ddots & \vdots \\ -\frac{c}{\beta_1} & 0 & \cdots & \frac{\mu_n+c}{\beta_n} - \hat{\lambda} \end{bmatrix},$$

where

$$\beta_1\Lambda = \mu_1 - \beta_1\hat{\lambda} + c\sum_{i=2}^n \frac{\mu_i - \beta_i\hat{\lambda}}{\mu_i + c - \beta_i\hat{\lambda}}.$$

Letting $P = 0$, we obtain eigenvalues $\{\hat{\lambda}_1, \ldots, \hat{\lambda}_n\}$, where $\hat{\lambda}_1$ is the solution to $(\beta_1\Lambda = 0)$ and $\hat{\lambda}_i = (\mu_i + nc)/\beta_i$ for $i = 2, \ldots, n$. Similarly, $\mathcal{R}_0 = 1/\min_i \hat{\lambda}_i$.

When $c \to \infty$, we have

$$\beta_1\Lambda \to \mu_1 - \hat{\lambda}\beta_1 + \sum_{i=2}^n(\mu_i - \beta_i\hat{\lambda}) = \sum_{i=1}^n \mu_i - \hat{\lambda}\sum_{i=1}^n \beta_i.$$

Thus, $\hat{\lambda}_1 \to \bar{\mu}/\bar{\beta}$, where $\bar{\beta}$ is the mean of all the regions' local infection rates. Furthermore, $\hat{\lambda}_i \to \infty$ for all $i \neq 1$. Therefore, $\mathcal{R}_0 \approx \bar{\beta}/\bar{\mu}$.

When $c \to 0$, $\hat{\lambda}_i \to \mu_i/\beta_i$ for all $i = 1, \ldots, n$, and $\mathcal{R}_0 \approx \max_i \beta_i/\mu_i$, i.e., the maximum basic reproduction number of the isolated regions.

APPENDIX C: PROOF OF THEOREM 4

Proof. Based on system (2), consider a possible Lyapunov function $V : \{X \in \Omega : S_i > 0, i = 1, \ldots, n\} \to \mathbb{R}$ by

$$V = \frac{1}{2}\left[\sum_{i=1}^n \left(S_i - N_i^S + I_i + R_i\right)\right]^2 + \sum_{i=1}^n I_i. \tag{C1}$$

Note that as S_i, I_i, and R_i approach infinity, the function V also approaches infinity, indicating that V is radially unbounded. Therefore, E^0 is the global minimum of V. Then the derivative of V along the trajectories of (2) is

$$V' = \sum_{i=1}^n \left(S_i - N_i^S + I_i + R_i\right)\frac{\mathrm{d}}{\mathrm{d}t}\sum_{i=1}^n (S_i + I_i + R_i) + \frac{\mathrm{d}}{\mathrm{d}t}\sum_{i=1}^n I_i.$$

Since there are no births/deaths in system (2), we have

$$\frac{\mathrm{d}}{\mathrm{d}t}\sum_{i=1}^n (S_i + I_i + R_i) = 0.$$

Therefore,

$$\begin{aligned} V' &= \sum_{i=1}^n \left(\beta_i\frac{I_iS_i}{N_i} - \mu_iI_i\right) \\ &= \sum_{i=1}^n \left[I_i(\beta_i\frac{S_i}{N_i} - \mu_i)\right] \\ &\leqslant I_{\max}\sum_{i=1}^n \left(\beta_i\frac{N_i^S}{N_i} + g - \mu_i\right), \end{aligned}$$

where $I_{\max}$ is the maximum I_i, and $g \geqslant 0$ is a parameter function that belongs to a bounded set associated with the network structure.

Rewriting V' in terms of a basic reproductive number, we have

$$V' \leqslant I_{\max}(\mathcal{R}_0 - 1),$$

where $\mathcal{R}_0 = \bar{\beta}/\bar{\mu} + g$.

If $\mathcal{R}_0 < 1$, then $V' \leqslant 0$. Note that $V' = 0$ if and only if $S_i = N_i^S$ and $I_i = 0$, or if $\mathcal{R}_0 = 1$, $S_i = N_i^S$, and $I_i = 0$ $(i = 1, \ldots, n)$. Therefore, the largest compact invariant set in $\{X \in \Omega : V' = 0\}$ is the singleton $\{E_0\}$, where E_0 is the disease-free equilibrium. According to LaSalle's invariant principle, E_0 is globally asymptotically stable.

[1] World Health Organization, Statement on the fifteenth meeting of the IHR (2005) Emergency Committee on the COVID-19 pandemic (2023).

[2] D. MacKenzie, *Stopping the Next Pandemic: How Covid-19 Can Help Us Save Humanity* (Bridge Street, London, 2021).

[3] H. Clark, M. Cárdenas, M. Dybul, M. Kazatchkine, J. Liu, D. Miliband, A. Nordström, P. Sudan, E. Zedillo, T. Obaid, R. McCarney, E. Radin, M. K. Eliasz, C. McNab, H. Legido-Quigley, and E. J. Sirleaf, The Lancet **399**, 1995 (2022).

[4] W. O. Kermack and A. G. McKendrick, Proc. R. Soc. A **115**, 700 (1927).

[5] H. W. Hethcote, Math. Biosci. **28**, 335 (1976).

[6] H. W. Hethcote and D. W. Tudor, J. Math. Biol. **9**, 37 (1980).

[7] R. Niu, E. W. M. Wong, Y.-C. Chan, M. A. van Wyk, and G. Chen, IEEE Access **8**, 195503 (2020).

[8] R. Niu, Y.-C. Chan, E. W. M. Wong, M. A. van Wyk, and G. Chen, Nonlin. Dyn. **106**, 1311 (2021).

[9] J. Wang, Y.-C. Chan, R. Niu, E. W. M. Wong, and M. A. van Wyk, Viruses **14**, 1482 (2022).

[10] P. Erdős and A. Rényi, Publ. Math. Debrecen **6**, 290 (1959).

[11] D. J. Watts and S. H. Strogatz, Nature (London) **393**, 440 (1998).

[12] A.-L. Barabási and R. Albert, Science **286**, 509 (1999).

[13] X. Fu, M. Small, and G. Chen, *Propagation Dynamics on Complex Networks: Models, Methods and Stability Analysis* (Wiley, Chichester, UK, 2013).

[14] M. E. J. Newman, Phys. Rev. E **66**, 016128 (2002).

[15] R. Pastor-Satorras and A. Vespignani, Phys. Rev. Lett. **86**, 3200 (2001).

[16] C. Granell, S. Gómez, and A. Arenas, Phys. Rev. Lett. **111**, 128701 (2013).

[17] X. Wei, X. Wu, S. Chen, J.-a. Lu, and G. Chen, SIAM J. Appl. Dyn. Syst. **17**, 1503 (2018).

[18] M. Ajelli, B. Gonçalves, D. Balcan, V. Colizza, H. Hu, J. J. Ramasco, S. Merler, and A. Vespignani, BMC Infectious Diseases **10**, 190 (2010).

[19] L. A. Rvachev and I. M. Longini Jr., Math. Biosci. **75**, 3 (1985).

[20] V. Colizza, R. Pastor-Satorras, and A. Vespignani, Nat. Phys. **3**, 276 (2007).

[21] J. Saldaña, Phys. Rev. E **78**, 012902 (2008).

[22] V. Colizza and A. Vespignani, J. Theor. Biol. **251**, 450 (2008).

[23] D. Balcan, V. Colizza, B. Gonçalves, H. Hu, J. J. Ramasco, and A. Vespignani, Proc. Natl. Acad. Sci. USA **106**, 21484 (2009).

[24] D. Juher, J. Ripoll, and J. Saldaña, Phys. Rev. E **80**, 041920 (2009).

[25] N. Masuda, New J. Phys. **12**, 093009 (2010).

[26] C. Shen, H. Chen, and Z. Hou, Phys. Rev. E **86**, 036114 (2012).

[27] A. Vespignani, Nat. Phys. **8**, 32 (2012).

[28] B. Wang, G. Tanaka, H. Suzuki, and K. Aihara, Phys. Rev. E **90**, 032806 (2014).

[29] Y.-W. Gong, Y.-R. Song, and G.-P. Jiang, Physica A **416**, 208 (2014).

[30] P. Valgañón, D. Soriano-Paños, A. Arenas, and J. Gómez-Gardeñes, Chaos **32**, 043102 (2022).

[31] D. Soriano-Paños, L. Lotero, A. Arenas, and J. Gómez-Gardeñes, Phys. Rev. X **8**, 031039 (2018).

[32] J. S. Brownstein, C. J. Wolfe, and K. D. Mandl, PLoS Med. **3**, e401 (2006).

[33] J.-B. Wang, L. Wang, and X. Li, IEEE Trans. Cybern. **46**, 2782 (2015).

[34] M. Chinazzi, J. T. Davis, M. Ajelli, C. Gioannini, M. Litvinova, S. Merler, A. Pastore y Piontti, K. Mu, L. Rossi, K. Sun *et al.*, Science **368**, 395 (2020).

[35] A. Arenas, W. Cota, J. Gómez-Gardeñes, S. Gómez, C. Granell, J. T. Matamalas, D. Soriano-Paños, and B. Steinegger, Phys. Rev. X **10**, 041055 (2020).

[36] S. Chang, E. Pierson, P. W. Koh, J. Gerardin, B. Redbird, D. Grusky, and J. Leskovec, Nature (London) **589**, 82 (2021).

[37] M. U. Kraemer, V. Hill, C. Ruis, S. Dellicour, S. Bajaj, J. T. McCrone, G. Baele, K. V. Parag, A. L. Battle, B. Gutierrez *et al.*, Science **373**, 889 (2021).

[38] J. M. Lee, D. Choi, G. Cho, and Y. Kim, J. Theor. Biol. **293**, 131 (2012).

[39] Z. Ruan, C. Wang, P. Ming Hui, and Z. Liu, Sci. Rep. **5**, 11401 (2015).

[40] N.-N. Wang, Y.-J. Wang, S.-H. Qiu, and Z.-R. Di, Commun. Nonlin. Sci. Numer. Simul. **109**, 106260 (2022).

[41] P. Castioni, R. Gallotti, and M. De Domenico, Commun. Phys. **4**, 131 (2021).

[42] M. Fiedler, Czech. Math. J. **23**, 298 (1973).

[43] X. F. Wang and G. Chen, Int. J. Bifurcation Chaos **12**, 187 (2002).

[44] S. Gomez, A. Diaz-Guilera, J. Gomez-Gardenes, C. J. Perez-Vicente, Y. Moreno, and A. Arenas, Phys. Rev. Lett. **110**, 028701 (2013).

[45] A. van der Schaft, Syst. Contr. Lett. **101**, 21 (2017).

[46] L. M. Pecora and T. L. Carroll, Phys. Rev. Lett. **80**, 2109 (1998).

[47] P. van den Driessche and J. Watmough, Math. Biosci. **180**, 29 (2002).

[48] Y.-Y. Gao and J.-A. Lu, Complex Syst. Complexity Sci. **9**, 38 (2012).

[49] A. Bigdeli, A. Tizghadam, and A. Leon-Garcia, in *Proceedings of the 1st Annual Workshop on Simplifying Complex Network for Practitioners* (ACM, New York, 2009), pp. 1–6.

[50] R. A. Rossi and N. K. Ahmed, in *Proceedings of the AAAI Conference on Artificial Intelligence, Vol. 29* (2015).

[51] A. Fronczak, P. Fronczak, and J. A. Hołyst, Phys. Rev. E **70**, 056110 (2004).

[52] E. Volz, J. Math. Biol. **56**, 293 (2008).

[53] Z. Li, B. Yang, J. Wang, Y. Wen, J. Xu, L. Ling, and T. Wang, Travel Med. Infectious Disease **52**, 102556 (2023).

[54] D. Lai, Y. Cai, T. H. Chan, D. Gan, A. N. Hurson, and Y. D. Zhang, BMJ Global Health **7**, e006975 (2022).